

Normal and Atypical Mitosis Image Classifier using Efficient Vision Transformer

Xuan Qi¹, Dominic Labella², Thomas Sanford³, and Maxwell Lee¹

¹Laboratory of Cancer Biology and Genetics, NCI, NIH, Bethesda, MD, 20852, USA

²Department of Radiation Oncology, Duke University Medical Center, Durham, NC, 27705, USA

³University of Hawaii Cancer Center, Honolulu, HI, 96813, USA

We tackle atypical versus normal mitosis classification in the MIDOG 2025 challenge using EfficientViT-L2, a hybrid CNN-ViT architecture optimized for accuracy and efficiency. A unified dataset of 13,938 nuclei from seven cancer types (MIDOG++ and AMi-Br) was used, with atypical mitoses comprising ~15%. To assess domain generalization, we applied leave-one-cancer-type-out cross-validation with 5-fold ensembles, using stain-deconvolution for image augmentation. For challenge submissions, we trained an ensemble with the same 5-fold split but on all cancer types. In the preliminary evaluation phase, this model achieved balanced accuracy of 0.859, ROC AUC of 0.942, and raw accuracy of 0.85, demonstrating competitive and well-balanced performance across metrics.

Mitosis Classification | Deep Learning | Pathology | EfficientViT

Correspondence: qix3@nih.gov

Supplementary Note 1: Background

A. datasets. We combined two officially provided datasets: Midog and Ami-Br into a single unified dataset and removed all duplicated samples to ensure data integrity. The final dataset comprises 13,938 annotated histopathology image samples spanning seven cancer types—four from canine tumors and three from human cancers, as summarized in Table 1. Each sample is labeled at the nucleus level as either Atypical Mitosis Figure (AMF) or Normal Mitosis Figure (NMF). Across the entire dataset, there exists very obvious class imbalance: AMF samples constitute only 8% to 24% of the nuclei within each cancer type, with an overall average of 15.6%. This imbalance poses a significant challenge for training robust classifiers and motivates the need for effective handling strategies such as data augmentation or class-weighted loss functions.

Cancer Type	Sample Num	AMF	NMF	AMF %
Canine cutaneous mast cell tumor	2327	351	1976	15.10%
Canine lung cancer	855	110	745	12.90%
Canine lymphoma	3959	317	3642	8.00%
Canine soft tissue sarcoma	1286	210	1076	16.30%
Human breast cancer	3722	832	2890	22.40%
Human melanoma	1150	271	879	23.60%
Human neuroendocrine tumor	639	85	554	13.30%
Total	13938	2176	11762	15.60%

Table 1. Distribution of AMF and NMF samples across different cancer types.

Supplementary Note 2: Methods

A. Efficient Vision Transformer (ViT). Vision Transformers (ViTs) are well suited for image classification as their self-attention mechanism captures long-range dependencies and global context from the very first layer, enabling integration of both fine-grained local features and broader structural cues. For mitosis classification, model efficiency is equally critical since whole-slide images contain millions of patches, requiring fast inference and low memory use to ensure practical deployment in clinical workflows. To address both accuracy and efficiency, we adopt EfficientViT (1), which combines convolutional and transformer modules in a hybrid architecture and employs cascaded linear attention to reduce computation and memory cost. Specifically, we use EfficientViT-L2 with a 256×256 input size, achieving 85.37% ImageNet accuracy with 64M parameters and 9.1 GMACs, offering an effective balance between performance and efficiency for large-scale mitosis classification.

B. Leave one out cross-validation (LOOCV) and model Ensemble. In real-world diagnostic settings, models often encounter unseen data that may differ significantly from the training data distribution. This challenge is especially relevant in our case, as the dataset used in this study includes only 7 cancer types, far fewer than the full spectrum of known cancers. To evaluate the generalization of our approach under such a practical and challenging scenario, we adopt a leave-one-out cross-validation (LOOCV) strategy. Specifically, we exclude one cancer type during training and use the remaining six for model development, testing the model’s performance on the held-out type.

Furthermore, for each LOOCV setting where the model is trained on data from 6 cancer types, we apply 5-fold cross-validation. In each fold, 4 subsets are used for training and 1 for validation, resulting in 5 trained models per LOOCV configuration. This yields a total of 7×5=35 models across all cancer types in this work. For evaluation on the held-out cancer type, we perform model ensembling by averaging the predicted AMF probability scores (ranging from 0.0 to 1.0) across the 5 models, using the mean confidence values as the final output.

Lastly, for final submission to preliminary and final stage of challenge, we train our ensemble model with same 5-fold split policy but on all cancer types data.

C. Data Augmentation and Other settings. For data augmentation, we follow the H&E stain based augmentation propose in (2). In this approach, image patches are first transformed into H&E color space via color deconvolution, after which each channel is perturbed independently by random scaling and shifting before being projected back to RGB. These controlled perturbations mimic realistic variations in stain intensity and hue while preserving tissue morphology, thereby exposing the network to a broader distribution of staining conditions.

For other deep learning related settings, we use weighted sampling for our data sampler, focal loss as loss function and AdamW as the optimizer.

Supplementary Note 3: Results

We first run our test with the LOOCV and 5-fold split settings mentioned in Section 1. Then, we submit our 5-fold ensemble model trained with all data to the preliminary eval phase of Midog 2025 challenge.

A. Performance metrics for LOOCV tests. We first plot the receiver operating characteristic (ROC) curves for each cancer type in Figure 1. As a threshold-independent metric, the ROC curve reflects the model’s ability to distinguish between AMF and NMF samples. Overall, the model demonstrates strong discriminative power, with consistently high AUC values across most cancer types.

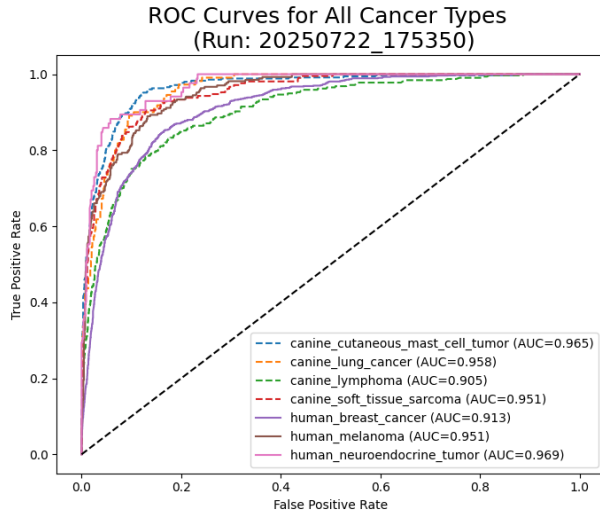


Fig. 1. ROC curves for testing all cancer types

For the BA score and confusion matrix, we adopt the Otsu thresholding (3) method to automatically determine the decision threshold for each cancer type in the test set. Otsu’s method is a ground-truth-free algorithm that selects an optimal threshold by maximizing the between-class variance in the prediction scores. This approach allows us to adaptively define thresholds without relying on manual tuning or label distribution assumptions, making it suitable for evaluating performance across imbalanced data or different cancer types.

Figure 2 presents the confusion matrices for each cancer type, showing class-wise prediction distributions after applying Otsu thresholding. These matrices provide insight into model bias and class-specific accuracy. Across most cancer types, AMF and NMF samples are well-separated, with high diagonal values indicating strong correct classification.

Table 2 summarizes the classification performance across cancer types using four metrics: ROC AUC, balanced accuracy (BA), NMF accuracy, and AMF accuracy. While ROC AUC reflects threshold-independent performance, the remaining metrics are calculated using thresholds automatically selected by the Otsu method.

Table 2. Performance metrics by cancer type

Cancer Type	ROC_AUC	BA	NMF_acc	AMF_acc
canine_cutaneous_mast_cell_tumor	0.965	0.909	0.894	0.923
canine_lung_cancer	0.958	0.873	0.928	0.818
canine_lymphoma	0.905	0.802	0.926	0.678
canine_soft_tissue_sarcoma	0.951	0.879	0.892	0.867
human_breast_cancer	0.913	0.830	0.777	0.882
human_melanoma	0.951	0.876	0.863	0.889
human_neuroendocrine_tumor	0.969	0.894	0.894	0.894

B. Preliminary Eval Phase result. In the preliminary evaluation phase, our model achieved consistent and well-balanced performance across all four domains. The average ROC AUC reached 0.942, demonstrating strong discriminative capability. The overall balanced accuracy was 0.859, highlighting stable performance across positive (AMF) and negative (NMF) classes. In addition, the model maintained a solid overall accuracy of 0.85, with sensitivity (0.873) and specificity (0.844) remaining well aligned.

Taken together, among high-ranked methods, our approach offers a well-balanced tradeoff across key evaluation metrics. Since the BA score is threshold dependent, it should be considered alongside threshold-independent ROC AUC, while raw accuracy provides additional context on overall performance. Under this comprehensive view, our method achieves competitive and well-balanced results across BA, ROC AUC, and raw accuracy. The raw eval results can be found (4) and ranking info can be found (5).

Table 3. Preliminary evaluation phase results across domains

Domain	ROC AUC	Accuracy	Sensitivity	Specificity	BA
Domain 0	0.875	0.806	1.000	0.781	0.891
Domain 1	0.898	0.820	0.724	0.841	0.783
Domain 2	0.974	0.888	0.972	0.854	0.913
Domain 3	0.972	0.895	1.000	0.889	0.944
Overall	0.942	0.850	0.873	0.844	0.859

1. Xinyu Liu, Houwen Peng, Ningxin Zheng, Yuqing Yang, Han Hu, and Yixuan Yuan. Efficientvit: Memory efficient vision transformer with cascaded group attention. In *Proceedings of the IEEE/CVF conference on computer vision and pattern recognition*, pages 14420–14430, 2023.
2. David Tellez, Maschenka Balkenhol, Nico Karssemeijer, Geert Litjens, Jeroen van der Laak, and Francesco Ciompi. H and e stain augmentation improves generalization of convolutional networks for histopathological mitosis detection. In *Medical Imaging 2018: Digital Pathology*, volume 10581, pages 264–270. SPIE, 2018.
3. Otsu’s method. Accessed: 28 August 2025.
4. Midog 2025 challenge – preliminary evaluation results, . Accessed: 2025-08-26.
5. Midog 2025 challenge – track 2 atypical mitosis classification preliminary leaderboard. Online, . Accessed: 2025-08-26.

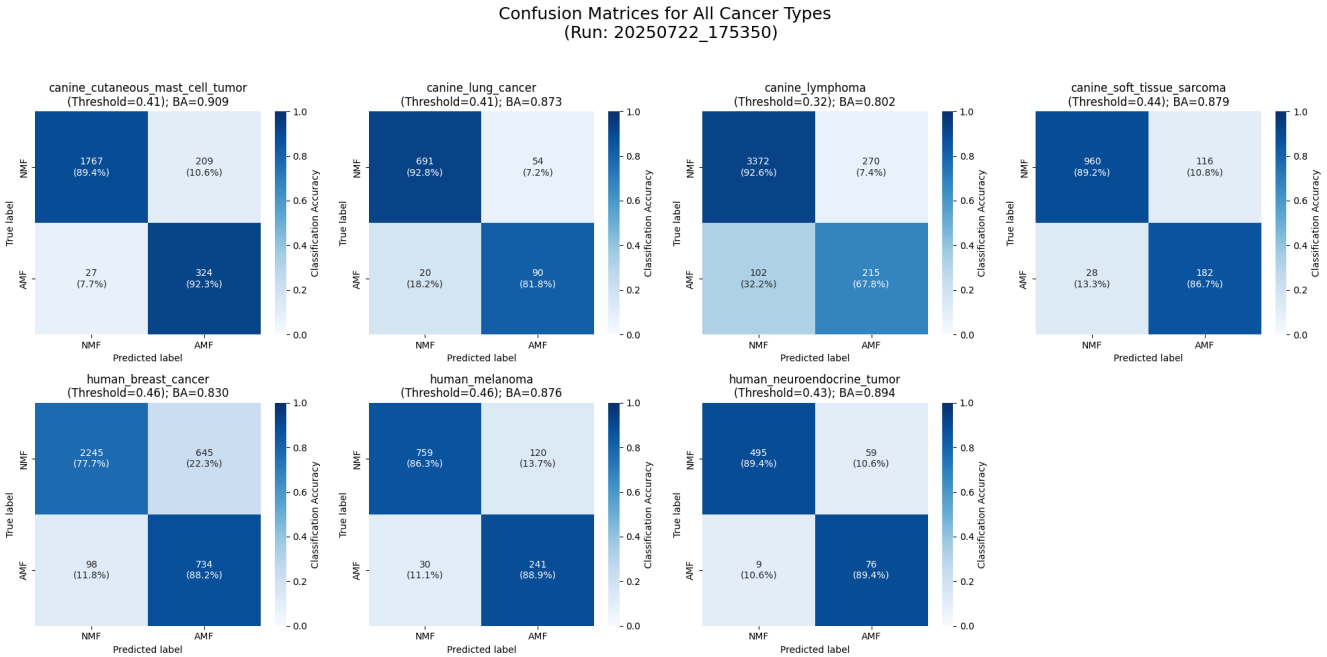


Fig. 2. Confusion matrix for testing all cancer types